

Higher energy electronic transitions of $\text{HC}_{2n+1}\text{H}^+$ ($n=2-7$) and HC_{2n+1}H ($n=4-7$) in neon matrices

Jan Fulara,^{1,2} Adam Nagy,¹ Iryna Garkusha,¹ and John P. Maier^{1,a)}

¹Department of Chemistry, University of Basel, Klingelbergstrasse 80, CH-4056 Basel, Switzerland

²Institute of Physics, Polish Academy of Sciences, Al. Lotników 32-46, PL-02668 Warsaw, Poland

(Received 3 April 2010; accepted 25 May 2010; published online 12 July 2010)

Electronic absorption spectra of linear $\text{HC}_{2n+1}\text{H}^+$ ($n=2-7$) were recorded in 6 K neon matrices following their mass-selective deposition. Four new electronic band systems are identified; the strongest $\tilde{\text{E}}^2\Pi_{g/u} \leftarrow \tilde{\text{X}}^2\Pi_{u/g}$ lies in the UV and the second most intense $\tilde{\text{C}}^2\Pi_{g/u} \leftarrow \tilde{\text{X}}^2\Pi_{u/g}$ is located in the visible range. The known $\tilde{\text{A}}^2\Pi_{g/u} \leftarrow \tilde{\text{X}}^2\Pi_{u/g}$ absorption is an order of magnitude weaker than $\tilde{\text{C}}^2\Pi_{g/u} \leftarrow \tilde{\text{X}}^2\Pi_{u/g}$. Transitions to the $\tilde{\text{B}}$ and $\tilde{\text{D}}$ states are also discussed. The wavelengths of the $\text{HC}_{2n+1}\text{H}^+$ ($n=2-7$) electronic systems obey a linear relation as a function of the size of the cations, similar to other carbon chains. The $\tilde{\text{B}}^3\Sigma_u^- \leftarrow \tilde{\text{X}}^3\Sigma_g^-$ transition in the UV of neutral HC_{2n+1}H ($n=4-7$) has also been identified upon photobleaching of the cations trapped in the matrices.

© 2010 American Institute of Physics. [doi:10.1063/1.3455208]

I. INTRODUCTION

Highly unsaturated hydrocarbon molecules, C_nH_m ($m=1, 2$), are important intermediates in terrestrial environments, such as in combustion under oxygen deficient conditions and discharges.¹ They are of astrophysical interest too as it is a well-established fact that the C_nH_m ($m=1, 2$) chains are constituents of the interstellar medium (ISM).^{2,3} Furthermore, they are perhaps building blocks of larger organic systems such as polycyclic aromatic hydrocarbons. C_nH ,⁴⁻⁷ C_nH^- ($n \leq 8$),⁸⁻¹⁰ and H_2C_n ($n \leq 6$) (Refs. 11-13) have been detected by their microwave transitions in many astronomical objects. Polyacetylenes, HC_{2n}H ($n=2, 3$), are also present in the ISM as their infrared bands were detected in carbon-rich protoplanetary nebulae.¹⁴

Particularly interesting are the n -odd members of the HC_nH series, because they are open-shell and their lowest energy electronic transition falls in the visible and near infrared. HC_{2n+1}H have been studied in the optical domain by direct absorption in neon¹⁵ and nitrogen¹⁶ matrices and in the gas phase by cavity ring-down^{17,18} and resonance enhanced multiphoton ionization methods.¹⁹ They were also studied by *ab initio* methods.²⁰⁻²⁴

Much less is known about the $\text{HC}_{2n+1}\text{H}^+$ ions. Apart from a few theoretical investigations on the smaller members of the $\text{HC}_{2n+1}\text{H}^+$ homologous series ($n=2-4$) (Refs. 25 and 26) there are only two reports on the spectroscopic studies of the lowest energy electronic transition of $\text{HC}_{2n+1}\text{H}^+$ ($n=2-7$).^{15,27} Recently, we explored higher energy electronic transitions of HC_{2n}H^+ ($n=2-7$) in neon matrices.²⁸ The results had encouraged us to come back to the spectroscopic studies of $\text{HC}_{2n+1}\text{H}^+$. In this contribution the higher

energy electronic transitions of $\text{HC}_{2n+1}\text{H}^+$ ($n=2-7$) and the UV transition of neutral HC_{2n+1}H ($n=4-7$) in neon matrices are reported.

II. EXPERIMENTAL

The apparatus used in the past²⁷ for mass-selective deposition of charged species into neon matrixes has been modified. All rubber seals in the matrix chamber were replaced with Cu gaskets and diffusion pumps by turbo ones. This improved the vacuum in the matrix chamber by more than one order of magnitude; the pressure is now below 1×10^{-8} mbar at room temperature. The monochromator and the photomultiplier/Si diode detectors have been replaced by a spectrograph with a focal length of 0.3 m, equipped with three gratings and a thermoelectrically cooled, open electrode charge coupled device (CCD) camera. The electronic absorption spectra are collected in several overlapping sections. The spectral width of a single section depends on the dimension of the active area of the CCD and resolution of the grating used.

The general idea for the detection of species trapped in a neon matrix remains nevertheless the same. Broadband light from a halogen or xenon lamp is focused on the entrance slit of the matrix and propagated ~ 2 cm through it in a “waveguide” mode. Light coming out of the matrix is focused onto a bundle of 50 optical fibers 1.0 mm in diameter. The output is shaped into a slit form (0.1×6 mm), which illuminates the entrance slit of the spectrograph.

In the present arrangement the light that probes the matrix during the recording of spectra has intensity several orders of magnitude higher than previously, where instead of broadband radiation, monochromatic light was used. Therefore, care was taken to minimize photoconversion of the species during the measurement. This was achieved by means of appropriate short-wavelength cutoff filters and by minimizing the exposure time of the matrix. The absorption spectra

^{a)}Author to whom correspondence should be addressed. FAX: +41-61-267-38-55. Electronic mail: j.p.maier@unibas.ch.

of the species were detected in several sections covering 220–1100 nm. The measurements were always started from the longest wavelength and they were continued into UV. The spectrum was then recorded again to test whether photoconversion of the species had taken place.

The $\text{HC}_{2n+1}\text{H}^+$ cations ($n=2-7$) were generated in a hot cathode discharge source from a mixture of diacetylene with helium; the ratio varied from 1:3 for the smaller cations ($n=2,3$) to 1:1 for the larger ones ($4 \leq n \leq 7$). The cations were separated in a quadrupole mass filter and the resolution of one mass unit was achieved for all ions but HC_{15}H^+ . In the latter case the resolution was slightly reduced to get sufficient ion current for the depositions. A picoammeter was used to measure the current during the matrix growth and by integration the total charge of the trapped $\text{HC}_{2n+1}\text{H}^+$ ions was evaluated. Under the best experimental conditions this was 29, 10, 13, 12, and 4 μC for $n=2-6$ for the deposition times 3.8, 2.3, 4.5, 5, and 5 h, respectively. For technical reasons, the ion current of HC_{15}H^+ could not be counted.

In order to suppress neutralization of the cations during deposition, a mixture of chloromethane with neon in a ratio of 1:20 000 was used to produce the host matrix. Chloromethane has a high electron affinity (~ 3 eV) and captures electrons efficiently forming Cl^- ions and CH_3 radicals.²⁹ The latter remain in matrix cages and due to the very low concentration they do not interfere with trapped cations, while Cl^- anions reduce the space charge. Moreover, neither of these species ($\text{CH}_3\text{Cl}, \text{CH}_3, \text{Cl}^-$) has absorption in the 200–1100 nm spectral range.

III. RESULTS AND DISCUSSION

A. $\tilde{A}^2\Pi_{g/u} \leftarrow \tilde{X}^2\Pi_{u/g}$ transition of $\text{HC}_{2n+1}\text{H}^+$ ($n=2-7$)

Deposition of the $\text{HC}_{2n+1}\text{H}^+$ cations ($n=2-7$) with neon led to the detection of several electronic band systems that extend from near infrared to UV. Figure 1 shows the lowest energy $\tilde{A}^2\Pi_b \leftarrow \tilde{X}^2\Pi_a$ transition of $\text{HC}_{2n+1}\text{H}^+$, where $a \equiv u$ and $b \equiv g$ for $n=\text{even}$ and vice versa for $n=\text{odd}$. This band system has already been reported,^{15,27} but is included here for two reasons. First, a higher signal-to-noise ratio was achieved and consequently more detail is seen in the spectra, e.g., vibrationally excited levels of HC_5H^+ and HC_7H^+ . The second was to compare its relative intensity with those of the newly observed transitions.

The $\tilde{A}^2\Pi_b \leftarrow \tilde{X}^2\Pi_a$ band systems of $\text{HC}_{2n+1}\text{H}^+$ ($n=2-7$) are similar in appearance. The origin band and a progression of ~ 2000 cm^{-1} that corresponds to the excitation of a $\text{C}\equiv\text{C}$ stretching mode in the \tilde{A} state are characteristic. Wavelengths of the bands in the $\tilde{A}^2\Pi_b \leftarrow \tilde{X}^2\Pi_a$ system are given in Table I. The origin band of $\text{HC}_{2n+1}\text{H}^+$ shifts monotonically by ~ 90 nm toward longer wavelengths as the size of cations increases, as shown earlier.²⁷ Another pattern observed is that the integrated intensity of the band system normalized to the same ion charge (1 μC) increases from 0.06 through 0.14, 0.32, and 0.37 to 0.86 in the series $n=2-6$.

The smaller members of the $\text{HC}_{2n+1}\text{H}^+$ series ($n=2-4$) have been studied by *ab initio* methods.^{25,26} The calculated

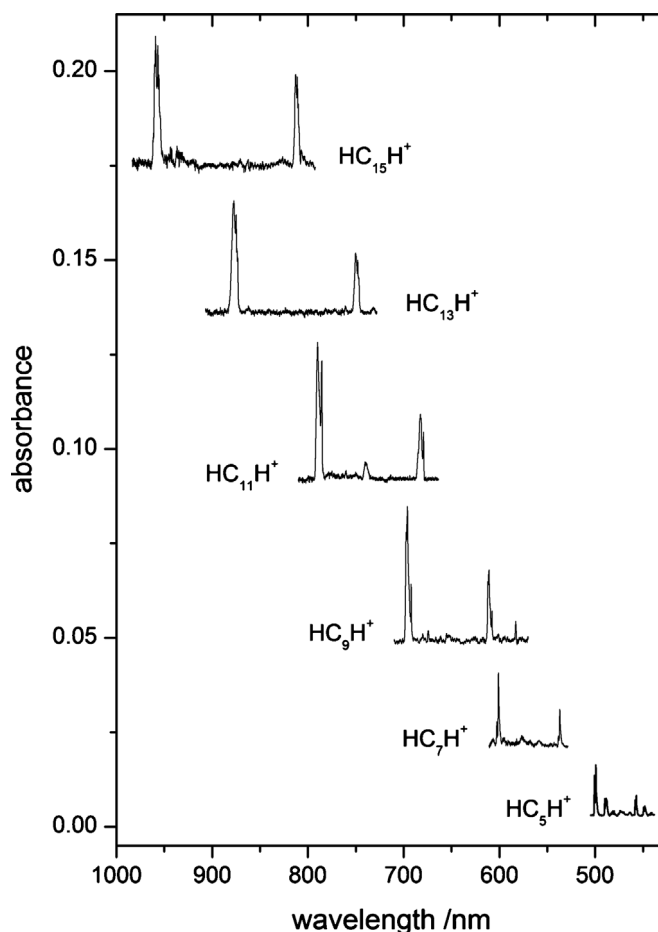


FIG. 1. The $\tilde{A}^2\Pi_{g/u} \leftarrow \tilde{X}^2\Pi_{u/g}$ electronic transition of $\text{HC}_{2n+1}\text{H}^+$ ($n=2-7$) in a neon matrix measured following deposition of mass-selected cations.

energy of the first allowed $\tilde{A}^2\Pi_b \leftarrow \tilde{X}^2\Pi_a$ transition is overestimated by 0.1–0.3 eV. The $\tilde{A}^2\Pi_b \leftarrow \tilde{X}^2\Pi_a$ transition of $\text{HC}_{2n+1}\text{H}^+$ can be classified as weak on the basis of its predicted oscillator strength ($f=0.004$, 0.002, and 0.007 for $n=2-4$, respectively). However, the calculations predict the f -values less accurately, e.g., the experimental integrated intensity of HC_7H^+ is 2.3 times larger than HC_5H^+ rather than two times weaker according to theory.

B. Visible spectral range

The $\text{HC}_{2n+1}\text{H}^+$ cations exhibit much richer electronic spectra than reported previously.^{15,27} Apart from the $\tilde{A}^2\Pi_b \leftarrow \tilde{X}^2\Pi_a$ transition, new absorptions are apparent in the visible and UV. The relative intensities of the bands seen in the visible (Fig. 2) for a given mass remain the same in experiments carried out under different conditions and they correlate well with the intensity of the $\tilde{A}^2\Pi_b \leftarrow \tilde{X}^2\Pi_a$ system (Fig. 1). This leads to the conclusion that absorptions seen in Figs. 1 and 2 originate just from one isomer, namely, linear $\text{HC}_{2n+1}\text{H}^+$.

The spectra of HC_5H^+ and HC_7H^+ shown in Fig. 2 are similar in appearance. Two bands (labeled B and C) dominate. They are separated from each other by 2813 and 2268 cm^{-1} for HC_5H^+ and HC_7H^+ . This spacing is too large to be assigned to vibrational excitation. Therefore, bands B

TABLE I. Observed band maxima ($\lambda \pm 0.1$ nm) in the electronic absorption spectra of $\text{HC}_{2n+1}\text{H}^+$ ($n=2-7$) and HC_{2n+1}H ($n=4-7$) in 6 K neon matrices with their suggested assignments.^a

Species	λ (nm)	$\tilde{\nu}$ (cm^{-1})	$\Delta\tilde{\nu}$ (cm^{-1})	Assignment ^b	
HC_5H^+	500.8	19 968	0	$0_0^0 \tilde{\text{A}}^2\Pi_g \leftarrow \tilde{\text{X}}^2\Pi_u$	
	490.0	20 408	440	$2\nu_8$	
	483.9	20 665	697	ν_3	
	481.5	20 768	800	$4\nu_8$	
	475.8	21 017	1049	$2\nu_9$	
	471.8	21 195	1227	$2\nu_7$	
	458.3	21 820	1852	ν_2	
	449.5	22 246	2278	$\nu_2+2\nu_8$	
	442.1	22 619	2651	$\nu_2+4\nu_8$	
	361.8	27 640	0	$0_0^0 \tilde{\text{B}}^2\Pi_g \leftarrow \tilde{\text{X}}^2\Pi_u$	
	355.2	28 153	513	$2\nu_8$	
	352.7	28 353	713	ν_3	
	350.0	28 571	931	$2\nu_{10}$	
	345.7	28 927	1287	$2\nu_7$	
	344.2	29 053	1413	$2\nu_3$	
	339.0	29 499	1859	ν_2	
	331.3	30 184	2544	$\nu_2+\nu_3$	
	328.1	30 479	0	$0_0^0 \tilde{\text{C}}^2\Pi_g \leftarrow \tilde{\text{X}}^2\Pi_u$	
	323.0	30 960	481	$2\nu_8$	
	320.3	31 221	742	ν_3	
	316.9	31 556	1077	$2\nu_9$	
	314.1	31 837	1358	$2\nu_7$	
	312.6	31 990	1511	$2\nu_3$	
	309.1	32 352	1873	ν_2	
	302.3	33 080	2601	$\nu_2+\nu_3$	
	292.5	34 188	3709	$2\nu_2$	
	HC_7H^+	599.8	16 672	0	$0_0^0 \tilde{\text{A}}^2\Pi_u \leftarrow \tilde{\text{X}}^2\Pi_g$
535.8		18 664	1992	ν_2	
448.4		22 302	0	$0_0^0 \tilde{\text{B}}^2\Pi_u \leftarrow \tilde{\text{X}}^2\Pi_g$	
437.5		22 857	555	ν_4	
428.7		23 326	1024	$2\nu_4$	
422.2		23 685	1383	ν_2	
411.4		24 307	2005	$0_0^0 \tilde{\text{C}}^2\Pi_u \leftarrow \tilde{\text{X}}^2\Pi_g$	
407.0		24 570	0	ν_4	
398.0		25 126	556	ν_2	
375.7		26 617	2047	$\nu_2+\nu_4$	
368.0		27 174	2604	$0_0^0 \tilde{\text{E}}^2\Pi_u \leftarrow \tilde{\text{X}}^2\Pi_g$	
231.8		43 141	0	$0_0^0 \tilde{\text{A}}^2\Pi_g \leftarrow \tilde{\text{X}}^2\Pi_u$	
HC_9H^+		694.9	14 391	0	$0_0^0 \tilde{\text{A}}^2\Pi_g \leftarrow \tilde{\text{X}}^2\Pi_u$
		609.9	16 396	2005	ν_3
	545.1	18 345	3954	$2\nu_3$	
	553.5	18 067	0	$0_0^0 \tilde{\text{B}}^2\Pi_g \leftarrow \tilde{\text{X}}^2\Pi_u$	
	539.3	18 543	476	ν_5	
	529.1	18 900	0	$0_0^0 \tilde{\text{C}}^2\Pi_g \leftarrow \tilde{\text{X}}^2\Pi_u$	
	517.2	19 335	435	ν_5	
	491.1	20 362	1462	ν_3	
	480.7	20 803	1903	ν_2	
	477.4	20 947	2047	$\nu_2+\nu_5$	
	467.7	21 381	2481	$\nu_2+\nu_5$	
	455.3	21 964	3064	$2\nu_3$	
	437.9	22 836	3936	$2\nu_2$	
	434.7	23 004	4104	$2\nu_2+\nu_5$	
	426.8	23 430	4530	$3\nu_2$	
	399.0	25 063	6163	$0_0^0+\delta \tilde{\text{D}}^2\Theta \leftarrow \tilde{\text{X}}^2\Pi_u$	
	323.5	30 912	$0+\delta$	ν_5	
	319.1	31 338	426	ν_4	
	316.7	31 576	664	$\nu_4+\nu_5$	
	312.3	32 020	1108	ν_3	
308.4	32 425	1513			
304.4	32 852	1940			

TABLE I. (Continued.)

Species	λ (nm)	$\tilde{\nu}$ (cm^{-1})	$\Delta\tilde{\nu}$ (cm^{-1})	Assignment ^b	
HC_9H	301.7	33 146	2234	$2\nu_4$	
	299.0	33 445	2533		
	295.5	33 841	2929		
	269.5	37 106	0	$0_0^0 \tilde{\text{E}}^2\Pi_g \leftarrow \tilde{\text{X}}^2\Pi_u$	
	266.6	37 509	403	ν_5	
	260.6	38 373	1267	ν_4	
	HC_{11}H^+	789.7	12 663	0	$0_0^0 \tilde{\text{A}}^2\Pi_u \leftarrow \tilde{\text{X}}^2\Pi_g$
		681.9	14 665	2002	ν_3
	HC_{11}H	598.3	16 714	4051	$2\nu_3$
		621.3	16 095	0	$0_0^0 \tilde{\text{B}}^2\Pi_u \leftarrow \tilde{\text{X}}^2\Pi_g$
605.6		16 513	418	ν_6	
615.1		16 258	0	$0_0^0 \tilde{\text{C}}^2\Pi_u \leftarrow \tilde{\text{X}}^2\Pi_g$	
547.2		18 275	2017	ν_3	
533.4		18 748	2490		
492.9		20 288	4030	$2\nu_3$	
366.3		27 300	$0+\delta$	$0_0^0+\delta \tilde{\text{D}}^2\Theta \leftarrow \tilde{\text{X}}^2\Pi_g$	
353.6		28 281	981	ν_5	
346.8		28 835	1535	ν_4	
342.2		29 223	1923	ν_3	
317.5		31 496	0	$0_0^0 \tilde{\text{E}}^2\Pi_u \leftarrow \tilde{\text{X}}^2\Pi_g$	
314.0		31 847	351	ν_6	
310.2		32 237	741	$2\nu_6$	
307.9		32 478	982		
305.5		32 733	1237	ν_5	
302.3		33 080	1584	$\nu_5+\nu_6$	
299.6		33 378	1882	ν_4	
294.2		33 990	2490	$2\nu_5$	
HC_{13}H^+		266.4	37 538	0	$0_0^0 \tilde{\text{B}}^2\Pi_u \leftarrow \tilde{\text{X}}^2\Pi_g$
	254.8	39 246	1708	ν_4	
	HC_{13}H	876.9	11 404	0	$0_0^0 \tilde{\text{A}}^2\Pi_g \leftarrow \tilde{\text{X}}^2\Pi_u$
		749.6	13 340	1936	ν_4
		659.2	15 170	3766	$2\nu_4$
		690.5	14 482	0	$0_0^0 \tilde{\text{C}}^2\Pi_g \leftarrow \tilde{\text{X}}^2\Pi_u$
		672.5	14 870	388	ν_7
		664.0	15 060	578	
		609.6	16 404	1922	ν_4
		542.5	18 433	3951	$2\nu_4$
490.1		20 404	5922	$3\nu_4$	
677.9		14 751	0	$0_0^0 \tilde{\text{B}}^2\Pi_g \leftarrow \tilde{\text{X}}^2\Pi_u$	
597.6		16 734	1983	ν_4	
406.0		24 631	$0+\delta$	$0_0^0+\delta \tilde{\text{D}}^2\Theta \leftarrow \tilde{\text{X}}^2\Pi_u$	
393.3		25 426	805		
390.8		25 589	958	ν_6	
382.0	26 178	1547	ν_5		
378.1	26 448	1817	ν_4		
366.2	27 307	0	$0_0^0 \tilde{\text{E}}^2\Pi_g \leftarrow \tilde{\text{X}}^2\Pi_u$		
362.3	27 601	294	ν_7		
359.2	27 840	533			
352.6	28 361	1054	ν_6		
350.7	28 514	1207			
347.7	28 760	1453	ν_5		
343.4	29 121	1814	ν_4		
340.4	29 377	2070	ν_3		
337.1	29 665	2358	$\nu_3+\nu_7$		
334.9	29 860	2553	$\nu_5+\nu_6$		
331.6	30 157	2850	$2\nu_5$		
325.5	30 722	3415	$\nu_3+\nu_5$		
313.7	31 878	4571			
303.4	32 960	5653			

TABLE I. (Continued.)

Species	λ (nm)	$\tilde{\nu}$ (cm ⁻¹)	$\Delta\tilde{\nu}$ (cm ⁻¹)	Assignment ^b
HC ₁₃ H	290.0	34 483	0	$0_0^0 \tilde{B}^3\Sigma_u^- \leftarrow \tilde{X}^3\Sigma_g^-$
	276.0	36 232	1749	ν_4
HC ₁₅ H ⁺	959.4	10 423	0	$0_0^0 \tilde{A}^2\Pi_u \leftarrow \tilde{X}^2\Pi_g$
	812.7	12 305	1882	ν_4 or ν_5
	702.7	14 231	3808	$2\nu_4$ or $2\nu_5$
	784.1	12 753	0	$0_0^0 \tilde{B}^2\Sigma_u^- \leftarrow \tilde{X}^2\Pi_g$
	711.3	14 059	1306	ν_6
	680.9	14 686	1933	ν_4
	603.8	16 562	3809	$2\nu_4$
	759.1	13 173	0	$0_0^0 \tilde{C}^2\Pi_u \leftarrow \tilde{X}^2\Pi_g$
	743.5	13 450	277	ν_8
	728.1	13 734	981	
	667.0	14 993	1820	ν_5
	661.0	15 129	1956	ν_4
	590.3	16 941	3768	$\nu_4 + \nu_5$
	585.8	17 071	3898	$2\nu_4$
	575.7	17 370	4197	$2\nu_4 + \nu_8$
	443.6	22 543	0 + δ	$0_0^0 + \delta \tilde{D}^2\Theta \leftarrow \tilde{X}^2\Pi_g$
	438.5	22 805	262	ν_8
	429.3	23 294	751	ν_7
	425.2	23 518	975	$\nu_7 + \nu_8$
	405.4	24 667	2124	ν_3
	398.8	25 075	0	$0_0^0 \tilde{E}^2\Pi_u \leftarrow \tilde{X}^2\Pi_g$
	393.5	25 413	338	ν_8
	389.8	25 654	579	
	384.7	25 994	919	ν_7
	381.0	26 247	1172	2×579
	378.8	26 399	1324	ν_6
	375.3	26 645	1570	
	371.6	26 911	1836	ν_5
368.3	27 152	2077	ν_4	
363.6	27 503	2428	$\nu_4 + \nu_8$	
354.0	28 249	3174	$\nu_5 + \nu_6$	
344.8	29 002	3927	$\nu_4 + \nu_5$	
332.7	30 057	4982		
HC ₁₅ H	313.1	31 939	0	$0_0^0 \tilde{B}^3\Sigma_u^- \leftarrow \tilde{X}^3\Sigma_g^-$
	297.8	33 580	1641	ν_5

^a σ_g^+ frequencies (in cm⁻¹) in the ground electronic state of HC_{2n+1}H⁺ calculated with DFT/B3LYP/cc-pVTZ: HC₅H⁺ 3383, 2052, 783; HC₇H⁺ 3400, 2135, 1698, 572; HC₉H⁺ 3413, 2155, 2064, 1275, 450; HC₁₁H⁺ 3430, 2156, 2143, 1791, 1070, 373; HC₁₃H⁺ 3436, 2195, 2124, 2057, 1461, 917, 317; HC₁₅H⁺ 3441, 2223, 2128, 2075, 1820, 1289, 802, 276.

^b Ξ and Θ : either Π or Φ symmetry (see text).

and C are assigned as the origins of two different electronic systems. MRD-CI calculations predict the excitation energy to the (2) $^2\Pi_g$ and (3) $^2\Pi_g$ electronic states of HC₅H⁺ at 3.75 and 3.85 eV, and at 3.14 and 3.17 eV to (2) $^2\Pi_u$ and (3) $^2\Pi_u$ of HC₇H⁺.²⁵ These values are quite near the energies of the B and C bands (3.43, 3.78 eV and 2.77, 3.05 eV) of the respective cations. However, the predicted oscillator strength to the (2) $^2\Pi$ state is 250 and 90 times smaller than to the (3) $^2\Pi$ state of HC₅H⁺ and HC₇H⁺, respectively, while the integrated intensity of system B is about two times lower than that of C for both cations. Weak bands lying on the high-energy side of B and C are assigned to vibrational excitation within the electronic transitions (Table I).

The absorption of HC₉H⁺ in the visible range is more alike those of the larger cations in the series than the smaller

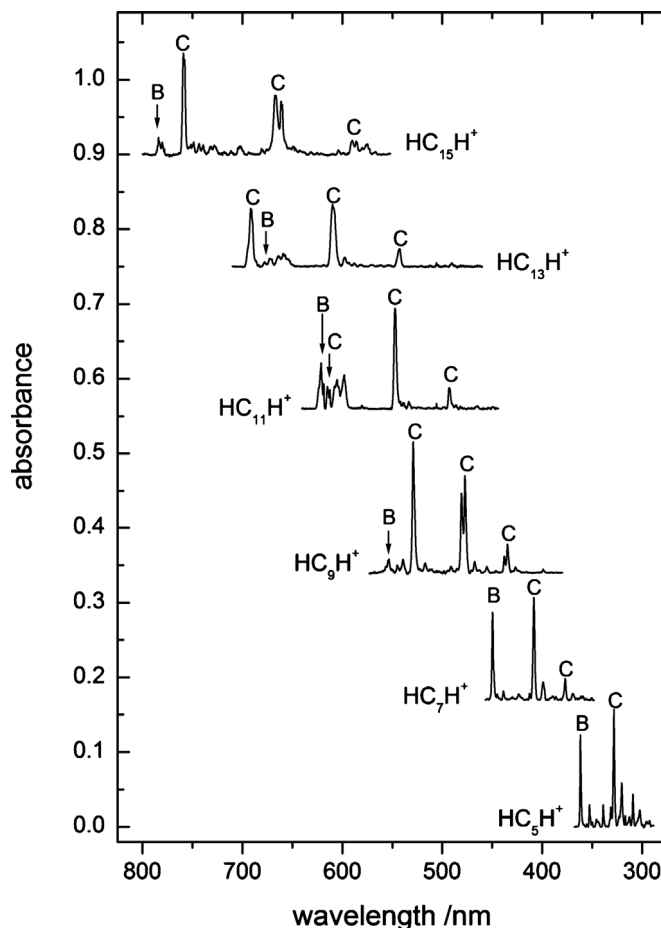


FIG. 2. Visible section of the spectra recorded following mass-selective deposition of HC_{2n+1}H⁺ ($n=2-7$) into a neon matrix. Two band systems marked with B and C are assigned to the $\tilde{B}^2\Pi_{g/u} \leftarrow \tilde{X}^2\Pi_{u/g}$ and $\tilde{C}^2\Pi_{g/u} \leftarrow \tilde{X}^2\Pi_{u/g}$ electronic transitions, respectively.

ones. A regular intensity distribution of the strongest bands (C in Fig. 2) is apparent. The most intense band lying on the lower energy edge of the spectrum is assigned as the onset of a new electronic transition. Other absorptions are due to two fundamental modes of energy 1903 and 2047 cm⁻¹ and their overtones, active in the excited electronic state. These are attributed to the ν_3 and ν_2 totally symmetric vibrations of HC₉H⁺ on the basis of DFT/B3LYP/cc-pVTZ calculations of the ground state frequencies for this cation, carried out using the GAUSSIAN 03 program suite.³⁰ Calculated energies of the σ_g^+ modes of the HC_{2n+1}H⁺ series ($n=2-7$) are included in the footnote of Table I.

In addition to the strong band system, the spectrum of HC₉H⁺ exhibits several weak absorptions at the low-energy side. In the visible spectral range, *ab initio* MRD-CI calculations locate three excited electronic states of symmetry (1) $^2\Phi_g$, (2) $^2\Pi_g$, and (3) $^2\Pi_g$ that are dipole accessible from the $\tilde{X}^2\Pi_u$ ground state of HC₉H⁺. The energies to these states are 2.48, 2.72, and 2.81 eV.²⁶ The strongest transition is to (2) $^2\Pi_g$ with an oscillator strength of 0.2. The transitions to the (1) $^2\Phi_g$ and (3) $^2\Pi_g$ states are predicted to be much weaker, with $f \sim 0.0004$ and 0.0001 , respectively. The origin band of the strong absorption system lies at 529.1 nm (2.34 eV) and the onset of the weaker one at 553.5 nm

(2.24 eV). The discrepancy between the calculated and experimental energies of the visible transitions of HC_9H^+ is larger (~ 0.5 eV) than for the smaller members of the same family. Because the energy levels of HC_9H^+ are predicted less accurately than for $\text{HC}_{2n+1}\text{H}^+$ ($n=2,3$) and as the (2) and (3) ${}^2\Pi_g$ states of HC_9H^+ lie close to each other according to theory, it is likely that their order is also reversed. In other words, the transition moment to the lower energy state (2) ${}^2\Pi_g$ is lower than to (3) ${}^2\Pi_g$. Therefore, we assign the strong band system of HC_9H^+ (C in Fig. 2) to the same $\tilde{C} {}^2\Pi_{g/uu}$ state as for the higher energy transitions of $\text{HC}_{2n+1}\text{H}^+$ ($n=2,3$).

The absorption spectra of HC_{13}H^+ and HC_{15}H^+ in the visible (Fig. 2) look much alike HC_9H^+ . Two band systems, the strong C one and the other, much weaker B, are discernible. The onset of the weak system \tilde{B} changes with respect to the origin band of the strong one \tilde{C} passing from HC_9H^+ to HC_{15}H^+ . In the case of HC_9H^+ it lies on the long-wavelength side of the origin of \tilde{C} , while for HC_{13}H^+ it is blueshifted, for HC_{15}H^+ it is again to the red. The electronic spectrum of HC_{11}H^+ (Fig. 2) has a peculiar appearance in comparison to the other members of the $\text{HC}_{2n+1}\text{H}^+$ series. The band at 547.2 nm dominates and a weaker one at 492.9 nm (separated by 2013 cm^{-1}) accompanies it. If one plots the wavelength of the origin band of the strong transition of $\text{HC}_{2n+1}\text{H}^+$ in the visible range as a function of the number of carbon atoms, a linear dependence is observed, as has been noted for the $\tilde{A} {}^2\Pi_b \leftarrow \tilde{X} {}^2\Pi_a$ transition and for other carbon chains.^{31,32} The band at 547.2 nm of HC_{11}H^+ departs considerably from this linear plot. This suggests that it is not the onset of the \tilde{C} transition. A common feature of the \tilde{C} band system of all the $\text{HC}_{2n+1}\text{H}^+$ cations is the appearance of a strong progression due to excitation of the $\text{C}\equiv\text{C}$ stretching modes. In this regard HC_{11}H^+ is not an exception, because a vibrational band of energy 2013 cm^{-1} is observed at 492.9 nm. Closer inspection of the moderately intense group of bands redshifted from the strongest (547.2 nm) locates a band at 615.1 nm, which is separated from the 547.2 nm peak by 2017 cm^{-1} . Therefore, the absorption at 615.1 nm is assigned as the onset of the \tilde{C} transition of HC_{11}H^+ ; the peak at 547.2 nm corresponds to the excitation of a fundamental and that at 492.9 nm is the overtone. The moderately intense group of bands around 620 nm is assigned to the weaker \tilde{B} transition. Proximity of the two electronic states \tilde{B} and \tilde{C} leads to interaction between them and as a result, weaker \tilde{B} transition gains in intensity. The \tilde{B} system of HC_{11}H^+ is therefore much stronger than observed for the other members of this series, while the origin band of \tilde{C} transition becomes exceptionally weak in comparison to the other $\text{HC}_{2n+1}\text{H}^+$ cations.

The strong \tilde{C} system of $\text{HC}_{2n+1}\text{H}^+$ ($n=5-7$) is assigned to the (3) ${}^2\Pi_b \leftarrow \tilde{X} {}^2\Pi_a$ transition by analogy to the smaller members ($n=2-4$) of this series, where $a\equiv u$ and $b\equiv g$ for $n=\text{even}$ and $a\equiv g$ and $b\equiv u$ for $n=\text{odd}$. The weaker system \tilde{B} can be assigned to the (2) ${}^2\Pi_b \leftarrow \tilde{X} {}^2\Pi_a$ transition; however, calculations for HC_9H^+ predict (1) ${}^2\Phi_g$ close to

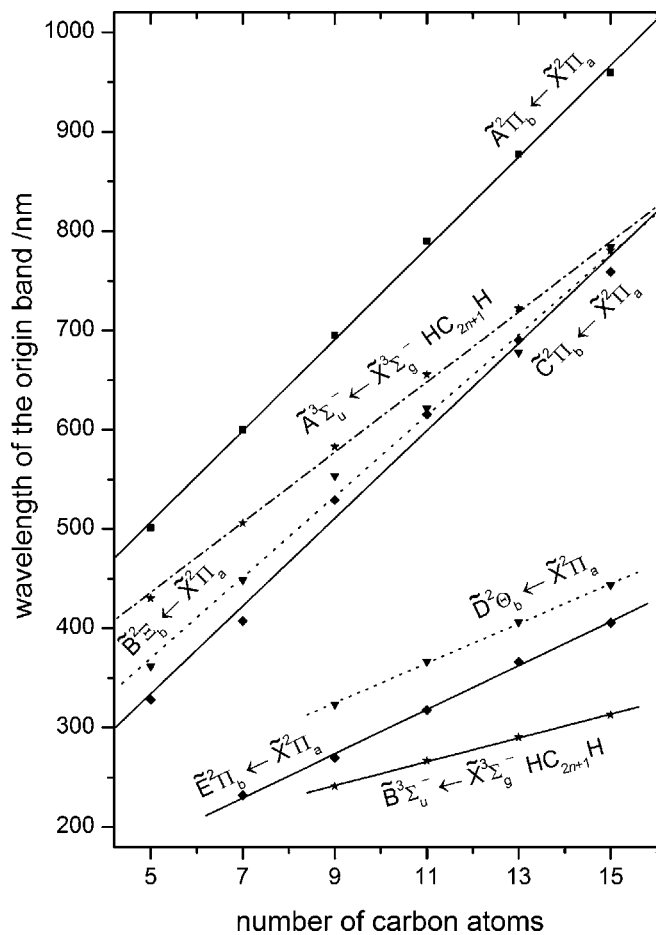


FIG. 3. Wavelengths of the origin band of electronic transitions of HC_{2n+1}H and $\text{HC}_{2n+1}\text{H}^+$ ($n=2-7$), plotted against the number of carbon atoms of the absorbing species.

(2) ${}^2\Pi_b$.²⁶ The symmetry of the \tilde{B} state is thus left open and the state is marked by Ξ in Table I, where Ξ denotes either Π or Φ . The wavelengths of the onset of the \tilde{B} and \tilde{C} transitions of $\text{HC}_{2n+1}\text{H}^+$ as a function of the number of carbon atoms lie on least squares fitted lines shown in Fig. 3. The linear fit for the \tilde{B} and \tilde{C} transition is somewhat worse than in case of $\tilde{A} {}^2\Pi_b \leftarrow \tilde{X} {}^2\Pi_a$ (regression coefficient R is 0.9958 and 0.9962 versus 0.9995). A reason could be interactions of \tilde{B} and \tilde{C} states due to their proximity.

C. UV spectral range

The UV section of the absorption spectra of $\text{HC}_{2n+1}\text{H}^+$ is shown in Fig. 4. For each cation but HC_7H^+ two spectra are shown: the upper one was recorded after deposition of mass-selected ions and the lower one after irradiation of the matrix with UV photons from a medium-pressure mercury lamp. One can distinguish absorptions that diminish upon irradiation and ones (marked by stars) which grow in intensity. The latter are due to neutral species.

Initially we focus on the region where the strongest absorptions of $\text{HC}_{2n+1}\text{H}^+$ ($n=3-7$) are. These are marked by letters a, c, e, g, and i in Fig. 4. Two band systems can be distinguished in the spectra. The first one (D) lies at lower wavelength and is weak, whereas the second one (E) bears

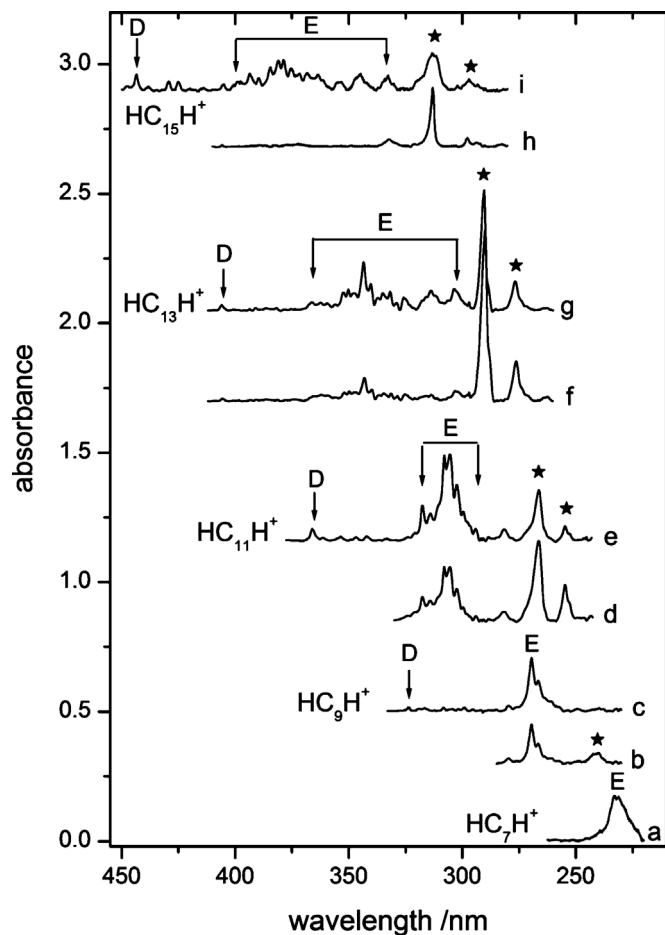


FIG. 4. UV range of the spectra of $\text{HC}_{2n+1}\text{H}^+$ ($n=2-7$) in a neon matrix. The ones marked with a, c, e, g, and i were measured after growing of the matrix. Those marked with b, d, and f were recorded after photobleaching with UV photons. The spectrum of HC_{15}H^+ (trace h) was recorded after matrix growth under continuous irradiation with UV photons from a medium pressure mercury lamp. Stars mark bands of neutral HC_{2n+1}H ($n=2-7$).

large intensity. In the case of HC_7H^+ there is a strong broad absorption centered at 231.8 nm, which rises steeply from lower wavelengths and then falls gradually. The short-wavelength edge of this band is obscured by scattered UV light in the matrix. For HC_9H^+ band E is shifted by ~ 38 nm toward red in comparison to HC_7H^+ and a multiplet structure is apparent. Band E of HC_{11}H^+ is shifted bathochromically by ~ 48 nm with respect to HC_9H^+ and the structure is even more evolved. This pattern is observed also for HC_{13}H^+ and HC_{15}H^+ . The E system of the latter cations spans over 60 nm and has a complex structure. If the wavelength of the E band of $\text{HC}_{2n+1}\text{H}^+$ ($n=3-5$) is plotted against the number of carbon atoms, the onset for HC_{13}H^+ and HC_{15}H^+ (vertical arrow on the left of the transition in Fig. 4) lies also on this line (Fig. 3).

Although the shape of system E changes on passing from HC_7H^+ to HC_{15}H^+ one can still assign it to the same electronic transition based upon the large intensity and the dependence of the wavelengths with size. For smaller $\text{HC}_{2n+1}\text{H}^+$ ($n=2-4$) members MRD-CI calculations predict a strong transition to the $(4) {}^2\Pi_b$ state ($b \equiv g, u, g$) at 7.02, 6.01, and 5.47 eV, respectively.^{25,26} The E band system for

HC_5H^+ was not observed, because according to the linear plot (Fig. 3) it should lie at ~ 188 nm, not accessible in our experiments. The experimental energy of E band system of HC_7H^+ is 5.35 eV, and 4.60 eV for HC_9H^+ . Therefore, we assign the E system to the $(4) {}^2\Pi_b \leftarrow \tilde{X} {}^2\Pi_a$ transition and label it as $\tilde{E} {}^2\Pi_b \leftarrow \tilde{X} {}^2\Pi_a$ to be consistent with the nomenclature used earlier in the text and in Figs. 3 and 4.

The vibronic structure of the $\tilde{E} {}^2\Pi_b \leftarrow \tilde{X} {}^2\Pi_a$ transition of $\text{HC}_{2n+1}\text{H}^+$ is more complex than for the lower energy ones. In the case of larger members ($n=6,7$) the transition extends 5000 cm^{-1} beyond the origin band. A weak origin band and the rich vibrational excitation are a signature of a geometry change in the $\tilde{E} {}^2\Pi_b$ excited with respect to the ground state. The suggested assignment to the σ_g^+ modes given in Table I is tentative.

A medium intensity band system (D in Fig. 4) lies to the red with respect to the \tilde{E} transition. The wavelength of this system versus the number of carbon atoms shows a linear dependence (Fig. 3) with $R=0.9996$. MRD-CI calculations for HC_7H^+ and HC_9H^+ predict several excited electronic states lying between the \tilde{C} and \tilde{E} states, but the transitions from the ground state to these are dipole-forbidden.^{25,26} It is difficult to deduce the \tilde{D} state symmetry and whether the transition appears because of vibronic interaction or if it is not adequately described by theory. This is left open and the \tilde{D} system is designated as $\tilde{D} {}^2\Theta_{a/b} \leftarrow \tilde{X} {}^2\Pi_a$, where ${}^2\Theta_{a/b}$ could be ${}^2\Pi$ or ${}^2\Phi$ and would have the same (a) or the opposite (b) to the ground state gerade/ungerade symmetry depending on whether it is vibronically induced or optically allowed transition, respectively. In Table I the onset of this transition is marked as $0_0^0 + \delta$, δ being the frequency of a nontotally symmetric vibration, while it equals 0 for the second case.

D. $\tilde{B} {}^3\Sigma_u^- \leftarrow \tilde{X} {}^3\Sigma_g^-$ transition of HC_{2n+1}H ($n=4-7$)

The bands of neutral HC_{2n+1}H ($n=4-7$) are identified in the UV region. They are marked with stars in the spectra recorded after deposition of mass-selected $\text{HC}_{2n+1}\text{H}^+$ (Fig. 4). They grow in intensity upon UV irradiation of the matrix. The spectra measured after photobleaching the $n=4-6$ members are denoted with letters b, d, and f in Fig. 4. The one marked h was recorded after continuous UV irradiation of the matrix during deposition of HC_{15}H^+ . The UV spectra of HC_{2n+1}H are simple as they exhibit two bands only: a strong origin and a weaker vibrational band lying $\sim 1700 \text{ cm}^{-1}$ above. In case of HC_9H only the origin band is seen in Fig. 4. The wavelengths of the of HC_{2n+1}H origin band of this transition follow a linear dependence as a function of the number of carbon atoms, similar to the known long-wavelength $\tilde{A} {}^3\Sigma_u^- \leftarrow \tilde{X} {}^3\Sigma_g^-$ transition¹⁵ (bottom and second from top lines in Fig. 3). Although the UV system of HC_{2n+1}H dominates the spectra shown in Fig. 4, the $\tilde{A} {}^3\Sigma_u^- \leftarrow \tilde{X} {}^3\Sigma_g^-$ transition is barely seen. In the case of HC_{11}H , where the strongest bands of the $\tilde{A} {}^3\Sigma_u^- \leftarrow \tilde{X} {}^3\Sigma_g^-$ system are discernible, the ratio of the integrated intensity of the UV band system to the visible one is evaluated to be

280 ± 30 . From the change of the intensity of neutral and ionic form of HC_{11}H upon UV irradiation one can also estimate the relative intensities of the strong UV transition of these species. They have an almost equal integrated intensity ($\text{HC}_{11}\text{H}/\text{HC}_{11}\text{H}^+ = 0.95 \pm 0.1$).

HC_{2n+1}H ($n=3-6,9$) have been studied in the gas-phase by means of a resonant two-color two-photon ionization technique.¹⁹ The wavelength of the origin band of HC_{13}H in the gas-phase is found at 281.82 nm and at 290.0 nm in a neon matrix. Smaller members of HC_{2n+1}H ($n=2-4$) have been studied by *ab initio* CASSCF and MRD-CI methods.^{19,22-24} These predict a strong transition from $\tilde{X}^3\Sigma_g^-$ to the $\tilde{B}^3\Sigma_u^-$ state. MRD-CI excitation to this state of HC_9H is at 5.91 eV,²³ while the present experimental data give 5.51 eV. The band system of HC_{2n+1}H ($n=4-7$) seen in Fig. 4 is assigned to the $\tilde{B}^3\Sigma_u^- \leftarrow \tilde{X}^3\Sigma_g^-$ electronic transi-

tion. The wavelengths of the observed bands of HC_{2n+1}H and their assignment are collected in Table I.

E. Comparison of the electronic transitions of $\text{HC}_{2n+1}\text{H}^+$ and HC_{2n}H^+ ($n=2-7$)

Even and odd members of the neutral HC_nH series differ considerably in their electronic structure due to the presence of a half-filled π orbital for the latter species. As a consequence, HC_{2n+1}H have triplet ground state in contrary to the singlet for evens. The lowest energy electronic transition of the odds falls into the visible and near infrared spectral ranges, while for the evens it lies in the UV. Other consequence is a triple/single bond alternation in the case of HC_{2n}H and a complex character for odd polyacetylenes. Theoretical studies reveal that the HC_{2n+1}H series splits into two subgroups (HC_{4n+1}H and HC_{4n+3}H) having similar geometri-

TABLE II. Comparison of electronic transition energies (in eV) of HC_{2n}H^+ (bold) and $\text{HC}_{2n+1}\text{H}^+$ ($n=2-7$) observed in a neon matrix with theoretical values (italic). Integrated intensities of these band systems and experimentally determined oscillator strengths are also included.

Species	Transitions					Label ^a
	$\tilde{A}^2\Pi \leftarrow \tilde{X}^2\Pi$	$\tilde{B}^2\Pi \leftarrow \tilde{X}^2\Pi$	$\tilde{C}^2\Pi \leftarrow \tilde{X}^2\Pi$	$\tilde{D}^2\Pi \leftarrow \tilde{X}^2\Pi$	$\tilde{E}^2\Pi \leftarrow \tilde{X}^2\Pi$	
HC_4H^+	2.44	...	3.69			ee
HC_5H^+	2.48	3.43	3.78			oe
	2.59	3.49	3.57			oc
	1.7	18	51			ii
	0.000 75	0.0076	0.022			f
HC_6H^+	2.05	...	2.97			ee
HC_7H^+	2.07	2.77	3.05	...	5.35	oe
	2.11	2.88	2.89			oc
	4.1	44	90		750 ^b	ii
	0.0018	0.019	0.039		0.32	f
HC_8H^+	1.74	2.18	2.50	...	5.11	ee
HC_9H^+	1.78	2.24	2.34	3.84	4.60	oe
	1.87	2.22	2.51			oc
	9.3	11	130	32	420	ii
	0.004	0.0046	0.057	0.014	0.18	f
HC_{10}H^+	1.51	1.91	2.19	...	4.50	ee
HC_{11}H^+	1.57	2.00	2.02	3.38	3.90	oe
	1.65	1.95	2.18			oc
	11	45	58	54	980	ii
	0.0046	0.020	0.025	0.023	0.43	f
HC_{12}H^+	1.33	1.70	...	2.30	4.01	ee
HC_{13}H^+	1.41	1.80	1.83	3.05	3.39	oe
	1.49	1.74	1.96			oc
	25	41	190	63	1850	ii
	0.11	0.018	0.081	0.027	0.79	f
HC_{14}H^+	1.18	1.54	...	2.03	3.62	ee
HC_{15}H^+	1.29	1.58	1.63	2.79	3.11	oe
	1.35	1.57	1.78			oc
	0.031	0.017	0.265	0.075	1.00 ^c	ii

^aee: experimental excitation energies of HC_{2n}H^+ (Ref. 28); oe experimental (this work) and oc calculated (Ref. 35) energies of $\text{HC}_{2n+1}\text{H}^+$; ii: integrated intensity (in 10^6 m mol^{-1}) of the systems; f: experimentally determined oscillator strengths.

^bIntegrated intensity of $\tilde{E}^2\Pi \leftarrow \tilde{X}^2\Pi$ is not corrected for broadening due to light scattering in the matrix.

^cIntensities are scaled to the strongest electronic transition $\tilde{E}^2\Pi \leftarrow \tilde{X}^2\Pi$, taken as 1.00.

cal structure.^{20,24,33} Such behavior can be expected also for cations of polyacetylenes, where both odd and even members have doublet ground state resulting from the unpaired π electron.^{20,24,33} Therefore, it is worthwhile to compare electronic transitions of even and odd members of the polyacetylene cations with each other.

Electronic transitions from the ground to higher excited electronic states of the even HC_{2n}H^+ ($n=2-7$) polyacetylene cation series have been studied in neon matrices.²⁸ These cations exhibit $\tilde{A}^2\Pi \leftarrow \tilde{X}^2\Pi$ electronic transition in the visible and near infrared and a strong $\tilde{E}^2\Pi \leftarrow \tilde{X}^2\Pi$ system in the UV. The intensity of the latter is an order of magnitude larger than that of the former. Three much weaker transitions to states \tilde{B} , \tilde{C} , and \tilde{D} lie between \tilde{A} and \tilde{E} in energy and have also been detected in these studies. Cations belonging to the odd $\text{HC}_{2n+1}\text{H}^+$ series mimic to some extent the even ones. The strongest electronic transition $\tilde{E}^2\Pi \leftarrow \tilde{X}^2\Pi$ lies also in the UV, the next most intense to state \tilde{C} is located in the visible range. The $\tilde{A}^2\Pi \leftarrow \tilde{X}^2\Pi$ transition is an order of magnitude weaker than the latter.

The energies of the electronic transitions of the even HC_{2n}H^+ and odd $\text{HC}_{2n+1}\text{H}^+$ series are compared in Table II. There is a striking similarity between the transition energy of two neighboring cations, e.g., HC_4H^+ and HC_5H^+ , ..., HC_{2n}H^+ , and $\text{HC}_{2n+1}\text{H}^+$. The origin bands of each such pair lie near each other. As we pointed out several years ago,²⁷ this regularity can be explained in the framework of the Hückel theory where such a pair of molecules has exactly the same excitation energy. Moreover, homologous series of linear chain molecules allows one to predict reliably the origin band of unknown members of the series. The linear dependence of the onsets of the electronic transitions on the number of carbon atoms in the case of $\text{HC}_{2n+1}\text{H}^+$ does not show any peculiarity that would support a difference between subgroups $\text{HC}_{4n+1}\text{H}^+$ and $\text{HC}_{4n+3}\text{H}^+$ (Fig. 3).

Recently, a paper on the excited electronic states of the odd-membered $\text{HC}_{2n+1}\text{H}^+$ series has appeared.³⁵ Energies of the first excited $\tilde{A}^2\Pi$ state for $n=2-7$ have been compared with experimental data for the long-wavelength $\tilde{A}^2\Pi \leftarrow \tilde{X}^2\Pi$ transition of these cations. A good agreement is apparent. The calculated excitation energies of $\text{HC}_{2n+1}\text{H}^+$ for higher-lying electronic states are also included in Table II. The predicted positions of the \tilde{B} and \tilde{C} states agree well with the present experimental data. Similar calculations have fit even better for the electronic states of the HC_{2n}H^+ cations.³⁴

F. Oscillator strengths of the electronic transitions of $\text{HC}_{2n+1}\text{H}^+$ ($n=2-6$)

Counting the total charge of the ions deposited into a neon matrix allows a comparison of electronic transition intensities. Integrated intensities of the band systems of $\text{HC}_{2n+1}\text{H}^+$ ($n=2-6$) are collected in Table II. The accuracy is estimated to be $\sim \pm 10\%$ within the same cation, while for two different species this could be somewhat worse. The integrated intensity of a given band system is proportional to the oscillator strength f of the transition. By knowing the

concentration of the cations trapped in the matrix and the optical path length, the f -values can be evaluated by using

$$f = \frac{4\varepsilon_0 m_e c^2 \ln 10}{N_A e^2} \int \varepsilon(\tilde{\nu}) d\tilde{\nu},$$

where f is the oscillator strength; ε_0 , m_e , c , N_A , and e are physical constants and $\varepsilon(\tilde{\nu})$ is the molar extinction coefficient. $\varepsilon(\tilde{\nu})$ can be evaluated from the number of cations deposited into the matrix (accumulated charge) and its volume ($2 \times 2 \times 0.015 \text{ cm}^3$). The path length was $\sim 2 \text{ cm}$.

To test how reliable f can be from the experimental data, the \tilde{A} , \tilde{B} , and \tilde{C} band systems of HC_5H^+ were chosen as for these the integrated intensities and the theoretical oscillator strengths resemble each other the most. The values obtained are $f(\tilde{A})=7.5 \times 10^{-4}$, $f(\tilde{B})=7.6 \times 10^{-3}$, and $f(\tilde{C})=0.022$, while calculations give 0.0005, 0.034, and 0.06, respectively.³⁵ Experiments provide a lower bound to oscillator strengths of cations because losses due to charge neutralization during deposition of the matrix are not taken into account. It is assumed that this can lower f by a factor of ~ 2 as the UV band system of neutral HC_{2n+1}H has an intensity comparable to the cationic one in the spectra recorded. The experimentally determined f -values for all the band systems for $\text{HC}_{2n+1}\text{H}^+$ are given in Table II.

The strong band systems of $\text{HC}_{2n+1}\text{H}^+$ and HC_{2n+1}H reported in this contribution provide more a sensitive means of detection of such species in gas-phase experiments and perhaps in astrophysical environments than it was possible via their weaker $\tilde{A}^2\Pi \leftarrow \tilde{X}^2\Pi$ or $\tilde{A}^3\Sigma_u^- \leftarrow \tilde{X}^3\Sigma_g^-$ transitions. In the case of $\text{HC}_{2n+1}\text{H}^+$ ($n=3-5$) most appropriate for this purpose is the $\tilde{E}^2\Pi \leftarrow \tilde{X}^2\Pi$ transition, while for the larger cations ($n=6,7$) more suitable is the $\tilde{C}^2\Pi \leftarrow \tilde{X}^2\Pi$ system.

ACKNOWLEDGMENTS

This work has been supported by the Swiss National Science Foundation (Project No. 200020-124349/1). We are grateful to L.O.T.-Oriol for lending us a Shamrock SR-303i spectrograph along with an iDus DV420A-OE CCD camera that enabled us to carry out these studies.

¹K.-H. Homann, *Angew. Chem., Int. Ed.* **37**, 2434 (1998) and references therein.

²M. B. Bell, P. A. Feldman, J. K. G. Watson, M. C. McCarthy, M. J. Travers, C. A. Gottlieb, and P. Thaddeus, *Astrophys. J.* **518**, 740 (1999).

³T. J. Millar, E. Herbst, and R. P. A. Bettens, *Mon. Not. R. Astron. Soc.* **316**, 195 (2000).

⁴M. Guélin, S. Green, and P. Thaddeus, *Astrophys. J.* **224**, L27 (1978).

⁵H. Suzuki, M. Ohishi, N. Kaifu, S. Ishikawa, and T. Kasuga, *Publ. Astron. Soc. Jpn.* **38**, 911 (1986).

⁶M. Guélin, J. Cernicharo, M. J. Travers, M. C. McCarthy, C. A. Gottlieb, P. Thaddeus, M. Ohishi, S. Saito, and S. Yamamoto, *Astron. Astrophys.* **317**, L1 (1997).

⁷J. Cernicharo and M. Guélin, *Astron. Astrophys.* **309**, L27 (1996).

⁸J. Cernicharo, M. Guélin, M. Agúndez, K. Kawaguchi, M. McCarthy, and P. Thaddeus, *Astron. Astrophys.* **467**, L37 (2007).

⁹M. C. McCarthy, C. A. Gottlieb, H. Gupta, and P. Thaddeus, *Astrophys. J.* **652**, L141 (2006).

¹⁰S. Brünken, H. Gupta, C. A. Gottlieb, M. C. McCarthy, and P. Thaddeus, *Astrophys. J.* **664**, L43 (2007).

¹¹J. Cernicharo, C. A. Gottlieb, M. Guélin, T. C. Killian, P. Thaddeus, and J. M. Vrtilek, *Astrophys. J. Lett.* **368**, L43 (1991).

¹²J. Cernicharo, C. A. Gottlieb, M. Guélin, T. C. Killian, G. Paubert, P.

- Thaddeus, and J. M. Vrtilik, *Astrophys. J. Lett.* **368**, L39 (1991).
- ¹³W. D. Langer, T. Velusamy, T. B. H. Kuiper, R. Peng, M. C. McCarthy, M. J. Travers, A. Kovács, C. A. Gottlieb, and P. Thaddeus, *Astrophys. J. Lett.* **480**, L63 (1997).
- ¹⁴J. Cernicharo, A. M. Heras, A. G. G. M. Tielens, J. R. Pardo, F. Herpin, M. Guélin, and L. B. F. M. Waters, *Astrophys. J.* **546**, L123 (2001).
- ¹⁵J. Fulara, P. Freivogel, D. Forney, and J. P. Maier, *J. Chem. Phys.* **103**, 8805 (1995).
- ¹⁶N. P. Bowling, R. J. Halter, J. A. Hodges, R. A. Seburg, P. S. Thomas, C. S. Simmons, J. F. Stanton, and R. J. McMahon, *J. Am. Chem. Soc.* **128**, 3291 (2006).
- ¹⁷C. D. Ball, M. C. McCarthy, and P. Thaddeus, *Astrophys. J.* **523**, L89 (1999).
- ¹⁸C. D. Ball, M. C. McCarthy, and P. Thaddeus, *J. Chem. Phys.* **112**, 10149 (2000).
- ¹⁹H. Ding, T. W. Schmidt, T. Pino, A. E. Boguslawskiy, F. Güthe, and J. P. Maier, *J. Chem. Phys.* **119**, 814 (2003).
- ²⁰R. A. Seburg, R. J. McMahon, J. F. Stanton, and J. Gauss, *J. Am. Chem. Soc.* **119**, 10838 (1997).
- ²¹L. Horný, N. D. K. Petraco, and H. F. Schaefer III, *J. Am. Chem. Soc.* **124**, 14716 (2002).
- ²²G. Mpourmpakis, M. Mühlhäuser, G. E. Froudakis, and S. D. Peyerimhoff, *Chem. Phys. Lett.* **356**, 398 (2002).
- ²³M. Mühlhäuser, J. Haubrich, and S. D. Peyerimhoff, *Chem. Phys.* **280**, 205 (2002).
- ²⁴C. Zhang, Z. Cao, H. Wu, and Q. Zhang, *Int. J. Quantum Chem.* **98**, 299 (2004).
- ²⁵M. Mühlhäuser, J. Haubrich, G. Mpourmpakis, A. Mavrandonakis, and G. E. Froudakis, *Internet Electron. J. Mol. Des.* **2**, 578 (2003).
- ²⁶M. Mühlhäuser, J. Haubrich, and S. D. Peyerimhoff, *Int. J. Quantum Chem.* **100**, 53 (2004).
- ²⁷P. Freivogel, J. Fulara, D. Lessen, D. Forney, and J. P. Maier, *Chem. Phys.* **189**, 335 (1994).
- ²⁸J. Fulara, M. Grutter, and J. P. Maier, *J. Phys. Chem. A* **111**, 11831 (2007).
- ²⁹Z. Y. Zhou, Y. M. Xing, and H. Gao, *J. Mol. Struct.: THEOCHEM* **542**, 79 (2001).
- ³⁰M. J. Frisch *et al.*, GAUSSIAN 03, Revision C.01, Gaussian, Inc., Pittsburgh, PA, 2003.
- ³¹P. Freivogel, J. Fulara, M. Jakobi, D. Forney, and J. P. Maier, *J. Chem. Phys.* **103**, 54 (1995).
- ³²D. Forney, P. Freivogel, J. Fulara, and J. P. Maier, *J. Chem. Phys.* **102**, 1510 (1995).
- ³³Q. Fan and G. V. Pfeiffer, *Chem. Phys. Lett.* **162**, 472 (1989).
- ³⁴J. Zhang, X. Guo, and Z. Cao, *J. Chem. Phys.* **131**, 144307 (2009).
- ³⁵J. Zhang, X. Guo, and Z. Cao, *Int. J. Mass. Spectrom.* **290**, 113 (2010).